Lymph compartment models and HIV intra patient infection dynamics

Steffi Knorn and Richard H. Middleton

***Abstract*— A compartment model is proposed to describe the HIV infection in humans. The compartments describe the blood, several lymph nodes and connecting lymph vessels. The dynamics in each compartment are described by a simplified HIV model considering the healthy and infected T-cells. A bifurcation analysis based on the variation of the proliferation rate is discussed and supported by simulations. Additional simulations illustrate the effect of a simple mutation model.**

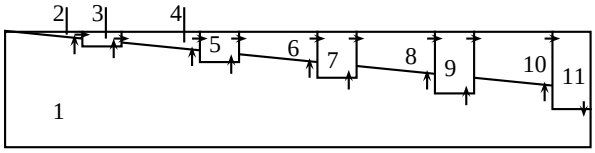

Fig. 1: Scheme of compartment model

I. Introduction

A variety of mathematical models of HIV infection have been examined with perhaps the earliest those in [1]–[3]. More recently, variants of these models (e.g. [4]) have been shown to exhibit several of the main traits of clinical observations of the disease. Most models only describe infection dynamics within the circulatory system. However, it is known that the lymphatic system plays an important role in the progression of HIV infection, e.g. [5], [6]. However, the lymphatic system exhibits some significant differences compared to the circulatory system:

An adult human body contains a huge number of small lymph capillaries, vessels and approximately 500–600 bean shaped lymph nodes varying in size up to approximately 1–2cm in diameter, [7]. Overall the adult human body contains approximately ten litres of lymph. The lymph flows are on-uniform and at a much slower rate than the blood.

More recently, the lymphatic system has been included in a three compartment HIV model in [8]. The compartments modelled are the blood, a remote region of the lymphatic system and an isolated sanctuary site. While Highly Active Anti-Retroviral Therapy (HAART) is assumed to be very efficient in the first compartment, it is much less efficient in the second and not efficient at all in the third compartment. The simulations in [8] revealed that due to the non uniform HAART efficiency, the viral load may be undetectable in the blood, whilst higher concentrations of virus persist in compartments 2 and 3.

This paper aims to extend these results. Due to the slow flow rate of the blood and the huge volume of lymph flowing in a very finely branched system it is unclear whether the lymphatic system can accurately be modelled as one single compartment as in [8]. Thus, we propose a model consisting of one compartment describing the blood and a chain of five lymph vessels alternating with five lymph nodes modelled as one compartment each. Despite the fact that lymph vessels are very thin, the overall volume of the finely branched system is much higher than the combined volume of all lymph nodes [7]. A rough estimation reveals that even assuming all 600 lymph nodes to be rather large, with a volume of $(10mm)^3$, they only contain approximately $600mL$ which is less than 10% of the overall lymphatic system.

The paper is organised as follows: The model and all modelling assumptions are discussed in Section II. A bifurcation analysis is presented in Section III. Section IV contains simulation results and interpretations thereof. The paper closes with discussions in Section V.

II. Model and Modelling Assumptions

A. Modelling Assumptions

The model used in this paper is a combination of the HIV model presented in [4] and an extension of the compartment model in [8]. Note that the description in [4] is a widely used model while [8] recently introduced a compartment model of the infected body.

Similar to [8] the system in this paper is assumed to be divided in several compartments. The first compartment represents the blood. The remaining compartments are parts of the lymphatic system. We assume that the lymphatic system consists of lymph vessels alternating with lymph nodes. The last compartment is a larger lymph vessel leading into a vein close to the heart. The volume of compartment i is denoted by V_i. We assume that the volumes are constant.

The pressure in the blood capillaries is higher than in the lymph capillaries. This causes blood plasma and some cells from the blood to be pushed into the lymph capillaries. These lead to lymph vessels of increasing size connecting lymph nodes of increasing size. The lymph vessel at the end of this chain (here the last compartment N) feeds into a vein close to the heart. The lymph only flows in one direction, i.e. from the capillaries towards the final vessel leading into the blood stream close to the heart. More details can be found in [7].

Thus, the concentration of cells in compartment i for lymph compartments (i.e. for $i = \{2,3,\ldots,N\}$) depends on the concentration of cells in compartment $i-1$ but not $i+1$.

Work supported by the Australian Research Council, grant number DP130103039

S. Knorn is with Signals and Systems Group at Uppsala University, Sweden, email: steffi.knorn@signal.uu.se; and R.H. Middleton is with the Centre for Complex Dynamic Systems and Control, The University of Newcastle, Australia, email: richard.middleton@newcastle.edu.au

The flow of lymph is very slow compared to the flow rate of blood. We assume that the lymph flow rate is approximately one metre per 6 days. We assume that there is a static flow of plasma / lymph and cells from the blood to each part of the lymphatic system.

Both flows are modelled as $v_{i-1}A_{i-1,i}$ and $v_{1,i}A_{1,i}$ where v_{i-1} is the lymph flow rate in compartment $i-1$ and $A_{i-1,i}$ is the effective area between compartments $i-1$ and i. For the flow from the blood into the lymph vessels the flow rate $v_{1,i}$ and the effective area $A_{1,i}$ are unknown.

To simplify and reduce the size of the model we use a simple HIV infection model consisting of healthy T-cells, denoted by T_i, and infected T-cells, denoted by T_i^*. T-cells are supplied by rate s_T in the thymus and then according to [9] discharged into the last lymph vessel that feeds into the heart. The T-cells and infected T-cells die with rates d_T and d_{T^*} respectively.

As in [4], in the case of an infection, the immune system is stimulated to multiply T-cells with rate ρ_i. This effect is known as infection induced proliferation. T-cells in compartment i get infected with rate constant β_i. Even if a lymph vessel and a lymph node of the same volume have the same concentration of healthy and infected T-cells, an infection is less likely in the vessel due to its shape. We therefore assume that the infection rate in the blood and the lymph nodes is much higher than the infection rate in the lymph vessels. Under HAART treatment ($u=1$) the infection rate in compartment i is reduced to $\beta_i(1-\eta\xi_i)$ where η is the efficiency of the drug and ξ_i its relative efficiency in compartment i.

B. Compartment model

Thus, the dynamics of the first compartment of the overall system (blood) can be described by

$$\begin{aligned}\dot{T}_1 =& -\underbrace{d_\mathrm{T}T_1}_{\text{death}} \underbrace{-\beta_1(1-u\eta\xi_1)T_1T_1^*}_{\text{infection}} \\ &+\underbrace{\frac{v_NA_{N,1}}{V_1}T_N}_{\text{inflow}} \underbrace{-\sum_{i=2}^{N}\frac{v_{1,i}A_{1,i}}{V_1}T_1}_{\text{outflow}} \underbrace{+\rho_1\frac{T_1T_1^*}{c+T_1^*}}_{\text{proliferation}}, \qquad (1)\\ \dot{T}_1^* =& -\underbrace{d_{\mathrm{T}^*}T_1^*}_{\text{death}} \underbrace{+\beta_1(1-u\eta\xi_1)T_1T_1^*}_{\text{infection}} \\ &+\underbrace{\frac{v_NA_{N,1}}{V_1}T_N^*}_{\text{inflow}} \underbrace{-\sum_{i=2}^{N}\frac{v_{1,i}A_{1,i}}{V_1}T_1^*}_{\text{outflow}}. \qquad (2)\end{aligned}$$

Similarly, the first lymph compartment, i.e. $i=2$, is modelled as

$$\begin{aligned}\dot{T}_2 =& -d_\mathrm{T}T_2-\beta_2(1-u\eta\xi_2)T_2T_2^*-\frac{v_2A_{2,3}}{V_2}T_2+\frac{v_{1,2}A_{1,2}}{V_2}T_1 \\ &+\rho_2\frac{T_2T_2^*}{c+T_2^*}, \qquad (3)\\ \dot{T}_2^* =& -d_{\mathrm{T}^*}T_2^*+\beta_2(1-u\eta\xi_2)T_2T_2^*-\frac{v_2A_{2,3}}{V_2}T_2^*+\frac{v_{1,2}A_{1,2}}{V_2}T_1^*. \qquad (4)\end{aligned}$$

The remaining lymph compartments for $i=\{3,4,\ldots,N-1\}$ are described by the differential equations

$$\begin{aligned}\dot{T}_i =& -d_\mathrm{T}T_i-\beta_i(1-u\eta\xi_i)T_iT_i^*+\frac{v_{i-1}A_{i-1,i}}{V_i}T_{i-1}-\frac{v_iA_{i,i+1}}{V_i}T_i \\ &+\frac{v_{1,i}A_{1,i}}{V_i}T_1+\rho_i\frac{T_iT_i^*}{c+T_i^*}, \qquad (5)\\ \dot{T}_i^* =& -d_{\mathrm{T}^*}T_i^*+\beta_i(1-u\eta\xi_i)T_iT_i^*+\frac{v_{i-1}A_{i-1,i}}{V_i}T_{i-1}^*-\frac{v_iA_{i,i+1}}{V_i}T_i^* \\ &+\frac{v_{1,i}A_{1,i}}{V_i}T_1^*. \qquad (6)\end{aligned}$$

The last lymph compartment is given by the model

$$\begin{aligned}\dot{T}_N =& s_\mathrm{T}-d_\mathrm{T}T_N-\beta_N(1-u\eta\xi_N)T_NT_N^*+\frac{v_{N-1}A_{N-1,N}}{V_N}T_{N-1} \\ &-\frac{v_NA_{N,1}}{V_N}T_N+\frac{v_{1,N}A_{1,N}}{V_N}T_1+\rho_N\frac{T_NT_N^*}{c+T_N^*}, \qquad (7)\\ \dot{T}_N^* =& -d_{\mathrm{T}^*}T_N^*+\beta_N(1-u\eta\xi_N)T_NT_N^*+\frac{v_{N-1}A_{N-1,N}}{V_N}T_{N-1}^* \\ &-\frac{v_NA_{N,1}}{V_N}T_N^*+\frac{v_{1,N}A_{1,N}}{V_N}T_1^*. \qquad (8)\end{aligned}$$

C. Simplifying Assumptions

The model can be simplified considerably using the assumptions that the lymph flow rate in all lymph vessels is equal, i.e. $v_i=v$ for all i. Together with the assumption that the volume of each compartment remains constant this yields $v_{1,i}A_{1,i}=v\,(A_{i,i+1}-A_{i-1,i})$ and $\sum_{i=2}^{N}v_{1,i}A_{1,i}=vA_{N,1}$ where v is the lymph flow rate of one metre per six days.

D. Simplified Compartment Model

Hence, the simplified system becomes

$$\begin{aligned}\underbrace{\begin{pmatrix}\dot{T}_1\\ \dot{T}_2\\ \dot{T}_3\\ \vdots\\ \dot{T}_N\end{pmatrix}}_{\dot{T}} =& -d_\mathrm{T}T-\underbrace{\begin{pmatrix}\beta_1(1-u\eta\xi_1)T_1T_1^*\\ \beta_2(1-u\eta\xi_2)T_2T_2^*\\ \beta_3(1-u\eta\xi_3)T_3T_3^*\\ \vdots\\ \beta_N(1-u\eta\xi_N)T_NT_N^*\end{pmatrix}}_{\phi_\beta}+\underbrace{\begin{pmatrix}\frac{\rho_1}{c+T_1^*}T_1T_1^*\\ \frac{\rho_2}{c+T_2^*}T_2T_2^*\\ \frac{\rho_3}{c+T_3^*}T_3T_3^*\\ \vdots\\ \frac{\rho_N}{c+T_N^*}T_NT_N^*\end{pmatrix}}_{\phi_\rho} \\ &+\begin{pmatrix}0\\0\\ \vdots\\0\\ s_\mathrm{T}\end{pmatrix}+v\underbrace{\begin{bmatrix}-\frac{A_{N,1}}{V_1} & 0 & 0 & \cdots & \frac{A_{N,1}}{V_1}\\ \frac{A_{2,3}}{V_2} & -\frac{A_{2,3}}{V_2} & 0 & \cdots & 0\\ \frac{A_{3,4}-A_{2,3}}{V_3} & \frac{A_{2,3}}{V_3} & -\frac{A_{3,4}}{V_3} & \ddots & 0\\ \vdots & 0 & \ddots & \ddots & 0\\ \frac{A_{N,1}-A_{N-1,N}}{V_N} & 0 & 0 & \frac{A_{N-1,N}}{V_N} & -\frac{A_{N,1}}{V_N}\end{bmatrix}}_{A_{\text{trans.}}}\underbrace{\begin{pmatrix}T_1\\T_2\\T_3\\ \vdots\\T_N\end{pmatrix}}_{T}\end{aligned} \qquad (9)$$

and

$$\dot{T}^* = -d_{\mathrm{T}^*}T^*+\phi_\beta+vA_{\text{trans.}}T^* \qquad (10)$$

where T^* is the vector of infected T-cells.

Description	Parameter	Value	Unit	Ref.
Blood	i_{B}	1	–	–
Lymph nodes	i_{LN}	{3,5,7,9,11}	–	–
Lymph vessels	i_{LV}	{2,4,6,8,10}	–	–
Death rate for T	d_{T}	0.01	$\frac{1}{\mathrm{day}}$	[4]
Death rate for T^*	d_{T^*}	0.3	$\frac{1}{\mathrm{day}}$	[4]
Infection in blood	β_1	$1.74 \cdot 10^{-3}$	$\frac{mm^3}{\mathrm{day}}$	[4]
Infection in lymph nodes	$\beta_{i_{\mathrm{LN}}}$	$1.74 \cdot 10^{-3}$	$\frac{mm^3}{\mathrm{day}}$	–
Infection in lymph vessels	$\beta_{i_{\mathrm{LV}}}$	$1.74 \cdot 10^{-5}$	$\frac{mm^3}{\mathrm{day}}$	–
Drug efficiency	η	0.9	–	[4]
Relative effic. in blood	ξ_i	1	–	[8]
Relative effic. in lymph	$\xi_{i_{\mathrm{LN}}}$, $\xi_{i_{\mathrm{LV}}}$	0.1	–	[8]
Prolifer. in blood	ρ_1	0	$\frac{1}{\mathrm{day}}$	–
Prolifer. in lymph nodes	$\rho_{i_{\mathrm{LN}}}$	{0,.1,.5,5}	$\frac{1}{\mathrm{day}}$	–
Prolifer. in lymph vessels	$\rho_{i_{\mathrm{LV}}}$	0	$\frac{1}{\mathrm{day}}$	–
50% prolifer. const.	c	3.45	$\frac{1}{mm^3}$	[4]
Supply rate for T	s	50000	$\frac{1}{mm^3 \mathrm{day}}$	[4]
Lymph flow rate	v	166.67	$\frac{mm}{\mathrm{day}}$	[9]

TABLE I: Parameter values for simplified model

E. Parameter Values

Note that most parameters have been adapted from a similar model presented in [4]. They can be found in Table I. The areas between the compartments (in mm^2) and the volumes of the compartments (in mm^3) are given by

$$\begin{bmatrix} A_{2,3} \\ A_{3,4} \\ \vdots \\ A_{10,11} \\ A_{11,1} \end{bmatrix} = \begin{bmatrix} 0.1 \\ 0.1001 \\ 0.1002 \\ 0.1003 \\ 0.1004 \\ 0.1005 \\ 0.1006 \\ 0.1007 \\ 0.1008 \\ 0.101 \end{bmatrix}, \quad \text{and} \quad \begin{bmatrix} V_1 \\ V_2 \\ \vdots \\ V_{11} \end{bmatrix} = \begin{bmatrix} 5 \cdot 10^6 \\ 1 \cdot 10^3 \\ 1 \cdot 10^3 \\ 7 \cdot 10^3 \\ 2 \cdot 10^3 \\ 15 \cdot 10^3 \\ 3 \cdot 10^3 \\ 20 \cdot 10^3 \\ 4 \cdot 10^3 \\ 40 \cdot 10^3 \\ 5 \cdot 10^3 \end{bmatrix}. \tag{11}$$

Note that similar to the compartment model in [8] the combined volume of all lymph compartments make up approximately one percent of the overall body volume modelled. Thus, only a small portion of the lymphatic system is considered exemplary. Due to simplifying modelling assumptions such as a constant flow rate of the lymph and constant volume of all compartments, the areas between the compartments have to increase very slowly to facilitate a small inflow of liquid from the blood system.

III. Bifurcation Studies

A. Simplified case without inflow of infected T-cells

This section aims to investigate the bifurcation of steady states in one single, simplified compartment model. Assume for simplicity the dynamics of one compartment can be described by

$$\dot{T} = s_{\mathrm{T}} - d_{\mathrm{T}} T - fT - \beta T T^* + \rho \frac{T T^*}{T^* + c}, \tag{12}$$

$$\dot{T}^* = -d_{\mathrm{T}^*} T^* - fT^* + \beta T T^*. \tag{13}$$

Note that s_{T} is the complete supply of healthy T-cells. This includes the supply from the Thymus, i.e. s, for one lymph compartment and inflow from other surrounding compartments. (The inflow of infected T-cells from surrounding compartments is neglected for simplicity. A perturbation analysis studying the case of a small inflow / supply of infected T-cells will be discussed in the next subsection.)

The outflow out of the compartment is modelled by fT and fT^* where f depends on the flow velocity v and the combined relative area towards neighbouring compartments as for instance in the fourth right hand term of (1). Note that the outflow rate affects both species in the same way but can vary between compartments. In contrast the death rates are different for healthy and infected T-cells but do not change in different compartments. Setting (13) to zero yields $\dot{T}^* = -d_{\mathrm{T}^*} T^* - fT^* + \beta T T^* = (\beta T - d_{\mathrm{T}^*} - f) T^* = 0$. Thus, the system has two equilibria. For the first one $T^*_{\mathrm{s},1} = 0$ and for the second $T_{\mathrm{s},2} = \frac{d_{\mathrm{T}^*} + f}{\beta}$. Substituting $T^*_{\mathrm{s},1} = T^*$ into (12) set to zero yields $T_{\mathrm{s},1} = \frac{s_{\mathrm{T}}}{d_{\mathrm{T}} + f}$. In order to study the stability of this equilibrium the system is linearised around the equilibrium. The linearised system becomes (where δ denotes a perturbation in a variable)

$$\begin{pmatrix} \delta\dot{T} \\ \delta\dot{T}^* \end{pmatrix} = \begin{bmatrix} -d_{\mathrm{T}} - f & -\frac{\beta s_{\mathrm{T}}}{d_{\mathrm{T}} + f} + \frac{\rho s_{\mathrm{T}}}{c(d_{\mathrm{T}} + f)} \\ 0 & -d_{\mathrm{T}^*} - f + \frac{\beta s_{\mathrm{T}}}{d_{\mathrm{T}} + f} \end{bmatrix} \begin{pmatrix} \delta T \\ \delta T^* \end{pmatrix} \tag{14}$$

The first eigenvalue at $-d_{\mathrm{T}} - f$ is negative as $d_{\mathrm{T}} > 0$ and $f > 0$. The second eigenvalue at $-d_{\mathrm{T}^*} - f + \frac{\beta s_{\mathrm{T}}}{d_{\mathrm{T}} + f}$ is negative for $\beta s_{\mathrm{T}} < (d_{\mathrm{T}^*} + f)(d_{\mathrm{T}} + f)$. Thus, this equilibrium (representing the uninfected body) is stable if and only if $\beta s_{\mathrm{T}} < (d_{\mathrm{T}^*} + f)(d_{\mathrm{T}} + f)$. Hence, if the infection rate or the supply is too high or the death and outflow rates too low, the equilibrium is unstable which means the infection is persistent.

Using $T_{\mathrm{s},2} = \frac{d_{\mathrm{T}^*} + f}{\beta}$ in (12) leads to

$$T^*_{\mathrm{s},2} = \frac{\alpha}{2(d_{\mathrm{T}^*} + f)\beta} - \frac{c}{2} + \frac{\rho}{2\beta} + \sqrt{\left(\frac{\alpha}{2(d_{\mathrm{T}^*} + f)\beta} - \frac{c}{2} + \frac{\rho}{2\beta}\right)^2 + c\frac{\alpha}{(d_{\mathrm{T}^*} + f)\beta}} \tag{15}$$

where $\alpha = \beta s_{\mathrm{T}} - (d_{\mathrm{T}^*} + f)(d_{\mathrm{T}} + f)$. Note that this equilibrium only exists for $\alpha > 0$ and therefore $\beta s_{\mathrm{T}} > (d_{\mathrm{T}^*} + f)(d_{\mathrm{T}} + f)$. Otherwise the equilibrium would be negative or complex. To study the stability of the second equilibrium the system is linearised around the equilibrium. The resulting matrix is

$$\begin{bmatrix} -d_{\mathrm{T}} - f - \beta T^*_{\mathrm{s},2} + \frac{\rho T^*_{\mathrm{s},2}}{T^*_{\mathrm{s},2} + c} & (d_{\mathrm{T}} + f)\left(\frac{c\rho}{\beta\left(T^*_{\mathrm{s},2} + c\right)^2} - 1\right) \\ \beta T^*_{\mathrm{s},2} & 0 \end{bmatrix}. \tag{16}$$

The eigenvalues of a 2×2 matrix are negative if

- the trace is negative: $-d_{\mathrm{T}} - f - \beta T^*_{\mathrm{s},2} + \frac{\rho T^*_{\mathrm{s},2}}{T^*_{\mathrm{s},2} + c} < 0$ is equivalent to $\rho < (d_{\mathrm{T}} + f)\frac{T^*_{\mathrm{s},2} + c}{T^*_{\mathrm{s},2}} + \beta T^*_{\mathrm{s},2} + \beta c$, and
- the determinant is positive: $-\beta T^*_{\mathrm{s},2}(d_{\mathrm{T}} + f)\left(\frac{c\rho}{\beta\left(T^*_{\mathrm{s},2} + c\right)^2} - 1\right) > 0$ implies $\rho < \frac{\beta\left(T^*_{\mathrm{s},2} + c\right)^2}{c}$.

Thus, for choices of ρ small enough the second equilibrium is stable. The exact upper bound of ρ depends on the equilibrium that depends on ρ itself. In case ρ does not satisfy the stability conditions, the equilibrium is unstable.

Note that this is a simplified model. For a more accurate analysis a supply rate of infected T-cells will be added in the following subsection.

B. Perturbation analysis for small inflow of infected T-cells

In case the concentration of infected T-cells is non zero in the neighbouring compartments, the dynamics of one compartment can be described by (12) and

$$\dot{T}^* = s_{\mathrm{T}^*} - d_{\mathrm{T}^*} T^* - f T^* + \beta T T^* \tag{17}$$

where s_{T^*} describes the combined, effective inflow of infected T-cells from neighbouring compartments. Assume that s_{T^*} is very slow, i.e. $s_{\mathrm{T}^*} = \varepsilon$.

It can be shown that, in this case, the first equilibrium is a perturbed version of the first, healthy equilibrium in Subsection III-A. Thus, $T^*_{\mathrm{s},1} = \frac{\varepsilon}{\beta T_{\mathrm{s},1} - d_{T^*} - f}$. Assume that ε is much smaller then $\beta T_{\mathrm{s},1} - d_{T^*} - f$ and we therefore can simplify $T^*_{\mathrm{s},1} \approx \varepsilon$. Then $T_{\mathrm{s},1} = \frac{s}{d_{\mathrm{T}} + f + \varepsilon(\beta - \frac{\rho}{\varepsilon + c})}$. It can be shown that the first eigenvalue of the linearised system matrix is approximately $-d_{\mathrm{T}} - f + \varepsilon(\beta - \frac{\rho}{\varepsilon + c})$. Since $d_{\mathrm{T}} + f > 0$ the eigenvalue will be negative for small perturbations ε. The second eigenvalue can be approximated by $-d_{\mathrm{T}^*} - f + \frac{\beta s_{\mathrm{T}}}{d_{\mathrm{T}} + f + \varepsilon(\beta - \frac{\rho}{\varepsilon + c})}$. Thus, for small perturbations and a low infection rate and supply of healthy T-cells compared to the combination of the death and outflow rates, the equilibrium is stable. Note that the compartment is "infected" as a small concentration due to the static inflow of unhealthy T-cells remains.

The perturbed second equilibrium can be approximated for small $s_{\mathrm{T}^*} = \varepsilon$ by

$$T^*_{\mathrm{s},2} = \frac{\alpha}{2(d_{\mathrm{T}^*} + f)\beta} - \frac{c}{2} + \frac{\rho}{2\beta} + \sqrt{\left(\frac{\alpha}{2(d_{\mathrm{T}^*} + f)\beta} - \frac{c}{2} + \frac{\rho}{2\beta}\right)^2 + c\frac{\alpha}{(d_{\mathrm{T}^*} + f)\beta} + \varepsilon\frac{d_{\mathrm{T}} + f - \rho}{(d_{\mathrm{T}^*} + f)\beta}} \tag{18}$$

where now we have $\alpha = \beta(s_{\mathrm{T}} + \varepsilon) - (d_{\mathrm{T}^*} + f)(d_{\mathrm{T}} + f)$. Note that again this equilibrium only exists for $\alpha > 0$ and therefore $\beta(s_{\mathrm{T}} + \varepsilon) > (d_{\mathrm{T}^*} + f)(d_{\mathrm{T}} + f)$. Otherwise the equilibrium would be negative or complex. It can further be shown that, similar to the unperturbed equilibrium, the perturbed equilibrium is stable for sufficiently small values of ρ.

It should be noted that the different compartments are coupled and the outflow of one compartment appears as a supply to another compartment. Hence, studying the bifurcation of a single isolated compartment can only give partial results. However, as we will see in the next section, this simplified analysis is still suitable to explain some results that can be observed in simulations.

IV. Simulation Results and Interpretations

A. The Effect of Virus Induced Proliferation of T Cells

In all scenarios we assume that the body is infected with a single infected T-cell in the blood after one year. Treatment is started one year after the infection.

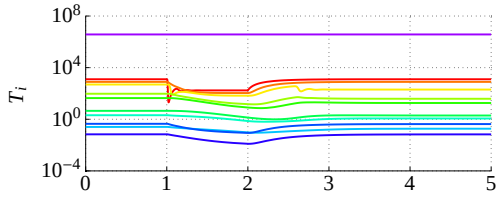

Fig. 2: Scenario 1 with $\rho_i = 0$ for all $i \in i_{\mathrm{LN}}$: T_i for $i = 1$ (red), 2 (orange), $\cdots$, N (purple)

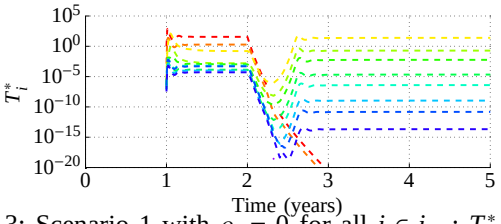

Fig. 3: Scenario 1 with $\rho_i = 0$ for all $i \in i_{\mathrm{LN}}$: T_i^* for $i = 1$ (red), 2 (orange), $\cdots$, N (purple)

In the first scenario assume that infection does not stimulate T-cell proliferation, i.e. $\rho_i = 0$ for all i. Using the approximate results from Section III we expect the infected equilibrium to be present for a sufficiently high infection rate and supply rate. It is stable (if it exists) since $\rho = 0$ and $c = 0$. Simulations in Fig. 2 and Fig. 3 reveal that upon infection the infected equilibrium is stable and the concentration of T settles to an equilibrium. After starting the treatment, β is reduced, leading to the change towards the heathy, now stable equilibrium. Hence, the concentration of T^* decreases. However, under the treatment, the concentration of T recovers. This leads to an increased supply of T in all compartments. As soon as the supply rate is high enough in some lymph compartments the infected, again stable equilibrium appears. Thus, the concentration of T^* increases again and settles to a new equilibrium. In some compartments the infected equilibrium after treatment is *higher* than the infected equilibrium without treatment such as in the 3rd, 4th and 5th compartment drawn in yellow, light green and green. Note that in the blood and the first lymph compartment the effective supply rate together with the reduced infection rate (due to the drug treatment) is low enough to maintain the healthy equilibrium.

In scenario 2, see Fig. 4 and Fig. 5, we assume that infection does stimulate T-cell proliferation in all lymph nodes of $\rho_i = 0.1$ for $i \in i_{\mathrm{LN}}$. Upon infection the system settles to the infected equilibrium that is stable in all compartments as ρ is small enough (or even 0) everywhere. As treatment is started the infection rate is reduced sufficiently in the blood for the healthy equilibrium to be stable. However, the lymph compartments remain at the infected equilibrium since the treatment is ineffective in the lymph system. This

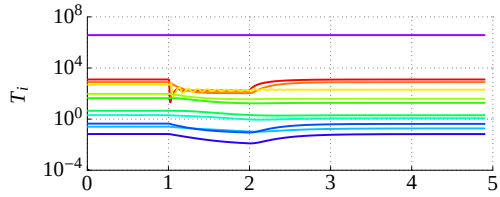

Fig. 4: Scenario 2 with $\rho_i = 0.1$ for all $i \in i_{\mathrm{LN}}$: T_i for $i = 1$ (red), 2 (orange), $\cdots$, N (purple)

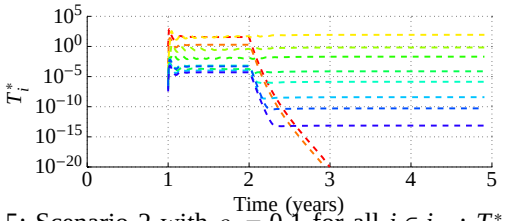

Fig. 5: Scenario 2 with $\rho_i = 0.1$ for all $i \in i_{\mathrm{LN}}$: T_i^* for $i = 1$ (red), 2 (orange), $\cdots$, N (purple)

equilibrium is shifted to a lower concentration of T^* in some lymph compartments while it remains almost unchanged in others. This behaviour cannot be fully explained using the bifurcation analysis in Section III as it seems to be influenced by the supply rate of T^* that has not been considered in the bifurcation analysis.

In scenario 3 the proliferation rate is further increased to $\rho_i = 0.5$ for $i \in i_{\mathrm{LN}}$. Simulations displayed in Fig. 6 and Fig. 7 reveal that even before commencing treatment the concentrations of healthy and infected T-cells start oscillating in some small compartments of the lymphatic system. This can be explained by observing that the infected equilibrium seems to be unstable in these compartments as ρ is too high. Thus, the states do not settle to the infected equilibrium but rather start oscillating. However, this effect does not cause significant infection of T-cells in the blood as T_1^* (red dashed line in Fig. 7) remains low. Here, the healthy equilibrium remains stable.

B. Allowing Simple Mutation

When allowing mutation of the wild type of the virus to a resistant variant the equations for $\dot{T}_i$ and $\dot{T}_i^*$ of each compartment are extended by adding the terms

$$-\beta_i T_i T_i^{\#} \quad \text{and} \quad +\mu\beta_i T_i T_i^{\#}, \tag{19}$$

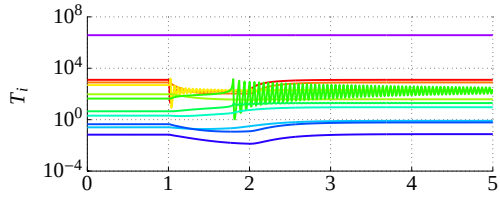

Fig. 6: Scenario 3 with $\rho_i = 0.5$ for all $i \in i_{\mathrm{LN}}$: T_i for $i = 1$ (red), 2 (orange), $\cdots$, N (purple)

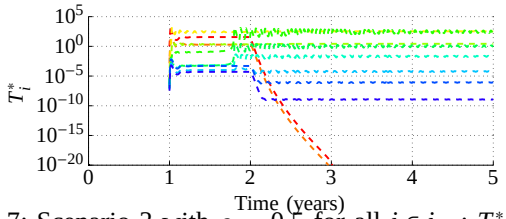

Fig. 7: Scenario 3 with $\rho_i = 0.5$ for all $i \in i_{\mathrm{LN}}$: T_i^* for $i = 1$ (red), 2 (orange), $\cdots$, N (purple)

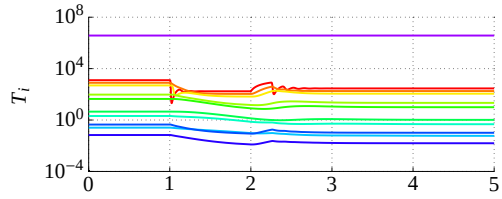

Fig. 8: Scenario 4 with $\rho_i = 0$ for all $i \in i_{\mathrm{LN}}$: T_i for $i = 1$ (red), 2 (orange), $\cdots$, N (purple)

respectively, where $T_i^{\#}$ is the concentration of T-cells infected with the mutant in compartment i and $\mu = 10^{-20}$ is the mutation coefficient. (Note that we take this extremely small value since we are assuming that at least 3 simultaneous mutations are required to confer resistance to all drugs in the combination ART). As we assume that the mutant is resistant to the treatment, the infection rate β_i here is not affected by the treatment or its relative efficiency in any compartment. For simplicity we assume β_i to be similar for the wild type and the mutant. To model a fitness advantage for the wild type over the mutant we assume that the death rate of the mutant is higher than that of the wild type: $d_{\mathrm{T}^{\#}} = 0.5/\mathrm{day}$.

In scenario 4 (shown in Fig. 8 and Fig. 9) a simple model without proliferation, i.e. $\rho_i = 0$ for all i, is simulated. The concentration of T-cells infected with the resistant mutant increases upon the start of treatment while the number of T-cells infected with the wild type decreases rapidly. The overall number of infected T-cells seem to be approximately the same as before starting treatment. Further work is needed for a detailed analysis of the system dynamics.

When setting the proliferation rate to $\rho_i = 0.1$ in scenario 5 (shown in Fig. 10 and Fig. 11) the concentration of T^* in most compartments (including the blood) decreases to a similar steady state value reached in scenario 4 (i.e. with $\rho_i =$

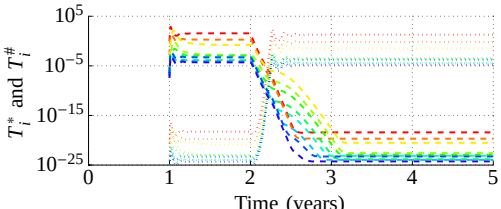

Fig. 9: Scenario 4 with $\rho_i = 0$ for all $i \in i_{\mathrm{LN}}$: T_i^* (dashed) and $T_i^{\#}$ (dotted) for $i = 1$ (red), 2 (orange), $\cdots$, N (purple)

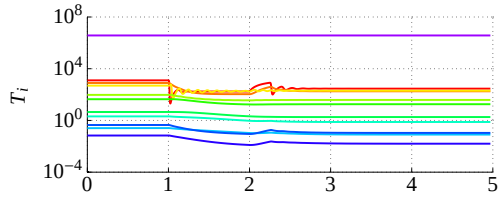

Fig. 10: Scenario 5 with $\rho_i = 0.1$ for all $i \in i_{\mathrm{LN}}$: T_i for $i = 1$ (red), 2 (orange), $\cdots$, N (purple)

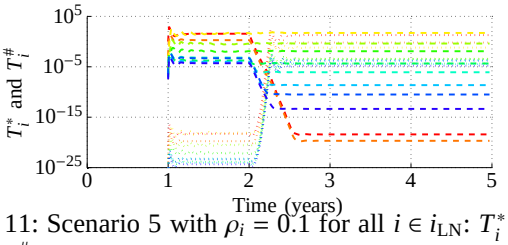

Fig. 11: Scenario 5 with $\rho_i = 0.1$ for all $i \in i_{\mathrm{LN}}$: T_i^* (dashed) and $T_i^\#$ (dotted) for $i = 1$ (red), 2 (orange), $\cdots$, N (purple)

0). However, in some small compartments of the lymphatic system the concentration of T^* remains almost unchanged upon the start of treatment despite the increased number of $T^\#$. The simulation results for the third compartment, i.e. the first and smallest lymph node, is shown in Fig. 12.

V. Discussions

In this work we have proposed a HIV model consisting of ten compartments describing several parts of the lymphatic system such as lymph nodes and vessels of different sizes and one compartment representing the blood. A simplified standard model has been used to describe the interaction between healthy and infected T-cells in each compartment. While the model in this paper and its parameters could not be validated, it is based on basic, known properties of the anatomy of the human body (such as size and structure of lymph vessels and nodes) and uses a well established model to describe the dynamics of healthy and infected T-cells.

A bifurcation analysis reveals that in the simplified model two equilibria (representing the healthy and infected case) might be present. It was shown that the existence of the infected equilibrium and its stability depend on system parameters such as death, supply, infection, flow and proliferation rate. The influence of the proliferation rate was

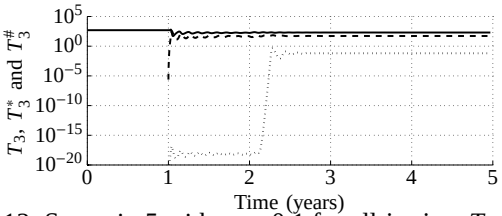

Fig. 12: Scenario 5 with $\rho_i = 0.1$ for all $i \in i_{\mathrm{LN}}$: T_3 (straight), T_3^* (dashed) and $T_3^\#$ (dotted)

examined by simulating different scenarios considering different proliferation rates. This revealed that the proliferation rate might play a vital role in the effect of HIV treatment.

It was also shown that within different body compartments different equilibria can be obtained. While in most simulated scenarios the concentration of infected T-cells in the blood under treatment approached zero, it settled on a nonzero value in most other compartments. In some cases the number of infected T-cells under treatment was higher than without treatment in some compartments of the body. Furthermore, in some cases interactions between model compartments led to changes of equilibria without a change of treatment.

These effects have so far usually been neglected in the existing body of work on HIV models. However, the authors believe that a better understanding of these compartments and their interactions might help to gain a better understanding of the infected body. In particular it might be potentially important to explain phenomena such as the rapid temporary increase of the viral load in the blood (known as viral "blips") currently not covered by the existing models.

Further investigations and simulations as well as a validation of the model are necessary to understand the role of proliferation and the overall lymphatic system in HIV infection and treatment. For instance, it is necessary (but potentially very difficult) to validate the model and the model parameters used to describe the dynamics in the lymphatic system. Further, it seems necessary to investigate whether a larger system with a more detailed network of lymph vessels and nodes leads to a significantly better model of the infected body. Using a more comprehensive HIV model (including for instance virus population, using different infection or proliferation models, allowing a supply of healthy T-cells in all compartment or considering a more detailed mutation model including crossover mutations among other extensions) might also lead to a better understanding of the role of the lymphatic system in HIV infection. A more detailed bifurcation analysis of the system might further help to understand the underlying dynamics.

References

[1] A. S. Perelson, D. E. Kirschner, and R. J. De Boer, "Dynamics of HIV infection of $CD4^+$ T cells," *Mathematical Biosciences*, vol. 114, 1993.

[2] M. A. Nowak and C. R. M. Bangham, "Population dynamics of immune responses to persistent viruses," *Science, New Series*, vol. 272, 1996.

[3] A. S. Perelson and P. W. Nelson, "Mathematical analysis of HIV-1 dynamics in vivo," *SIAM review*, vol. 41, no. 1, pp. 3–44, 1999.

[4] E. A. Hernandez-Vargas and R. H. Middleton, "Modeling the three stages in HIV infection," *Journal of Theoretical Biology*, vol. 320, 2013.

[5] G. Pantaleo, O. Cohen, T. Schacker, M. Vaccarezza, C. Graziosi, P. Rizzardi, J. Kahn, C. Fox, S. Schnittman, D. Schwartz, L. Corey, and A. Fauci, "Evolutionary pattern of human immunodeficiency virus (HIV) replication and distribution in lymph nodes following primary infection: Implications for antiviral therapy," *Nature Medicine*, 1998.

[6] R. J. De Boer, R. M. Ribeiro, and A. S. Perelson, "Current Estimates for HIV-1 Production Imply Rapid Viral Clearance in Lymphoid Tissues," *PLoS Computational Biology*, vol. 6, no. 9, 2010.

[7] P. L. Williams, R. Warwick, M. Dyson, and L. H. Bannister, Eds., *Gray's Anatomy*, 37th ed. Churchill Livingstone, 1989.

[8] E. Cardozo, C. Vargas, and R. Zurakowski, "A Compartment Based Model for the formation of 2-LTR Circles after Raltegravir Intensification," in *51st IEEE Conference on Decision and Control*, 2012.

[9] R. J. Cano and J. S. Colomé, *Essentials of Microbiology*. West Publishing Company, 1988.